Transcranial photoacoustic imaging of NMDA-evoked focal circuit dynamics in rat forebrain

Jeeun Kang[1, 2], Shilpa D. Kadam[3], Joshua S. Elmore[1], Brennan J. Sullivan[4,*], Heather Valentine[1,*], Adarsha P. Malla[5], Maged M. Harraz[5], Arman Rahmim[1], Jin Kang[2, 6], Leslie M. Loew[7], Michael Baumann[8], Anthony A. Grace[9], Albert Gjedde[1,10,11,12], Emad M. Boctor[1,2,6, 13,†], Dean F. Wong[1,5,14,15 †]

[1] Russell H. Morgan Department of Radiology and Radiological Science, Johns Hopkins University, Baltimore, MD, USA.

[2] Laboratory of Computational Sensing and Robotics, Whiting School of Engineering, Johns Hopkins University, Baltimore, MD, USA

[3] Neuroscience Laboratory, Hugo W. Moser Research Institute at Kennedy Krieger & Department of Neurology, Johns Hopkins Medical Institutions, Baltimore, MD, USA

[4] Neuroscience Laboratory, Hugo W. Moser Research Institute at Kennedy Krieger, Baltimore, MD, USA

[5] The Solomon H. Snyder Department of Neuroscience, Johns Hopkins University School of Medicine, Baltimore, MD, USA

[6] Department of Electrical and Computer Engineering, Whiting School of Engineering, Johns Hopkins University, Baltimore, MD, USA

[7] Department of Cell Biology, University of Connecticut Health, Farmington, CT, USA

[8] National Institute on Drug Abuse, Intramural Research Program, NIH, Baltimore, MD

[9] Departments of Neuroscience, Psychiatry and Psychology, University of Pittsburgh, Pittsburgh, PA, USA

[10] Department of Neurology and Neurosurgery, McGill University, Montreal, Quebec, Canada

[11] Departments of Clinical Research and Nuclear Medicine, Odense University Hospital and University of Southern Denmark, Odense, Denmark

[12] Department of Neuroscience, University of Copenhagen, Copenhagen, Denmark

[13] Department of Computer Science, Whiting School of Engineering, Johns Hopkins University, Baltimore, MD, USA

[14] Department of Psychiatry and Behavioral Sciences, Johns Hopkins Medical Institutions, Baltimore, MD, USA

[15] Department of Neurology, Johns Hopkins Medical Institutions, Baltimore, MD, USA

*** Equal contribution**

† These authors share senior authorship and address all correspondence to: Dean F. Wong, E-mail: dfwong@jhmi.edu and to Emad M. Boctor, E-mail: eboctor1@jhmi.edu;

Keywords: Photoacoustic, neuroimaging, voltage-sensitive dye imaging, microdialysis, quantitative encephalopathy, N-methyl-D-aspartate, glutamate, motor cortex, hippocampus

Abstract

Transcranial photoacoustic (PA) voltage-sensitive dye (VSD) imaging promises to overcome current temporal and spatial limitations of functional neuroimaging. The technique previously distinguished global seizure activity from control neural activity in groups of rats. To validate the focal specificity of transcranial PA with VSD (IR780) imaging *in vivo*, we now present proofs-of-concept that the results differentiate between N-methyl-D-aspartate (NMDA) evoked neural activities in two distinct circuits with differential response profiles, i.e., sensorimotor cortex and hippocampus. Concurrent quantitative EEG (qEEG) recorded real time circuit dynamics. We hypothesized that NMDA evoked focal glutamate release in both circuits would correlate with increases of location-specific PA signals and time-specific EEG signals.

To test the hypothesis in hippocampus, we infused 0.3, 1, and 3 mM NMDA at 2 μl/min over 60 min via an implanted microdialysis probe. The dialysate samples collected every 20 minutes during the infusion were analyzed for focal changes in extracellular glutamate release and quantified by high-performance liquid chromatography (HPLC). Microdialysis at 0.3, 1, and 3 mM showed dose-dependent increases of glutamate (39%, 200% and 670 %, respectively) in hippocampus. We recorded dose-dependent increases of the PA signal with 0.3 and 3 mM NMDA infusion as predicted. Quantitative EEG at 3 mM NMDA infusion confirmed induction of focal seizure activity. Transcranial PA VSD imaging provided up to 301±42% of fractional neural activity index change measured at the contralateral side of the microdialysis probe with 3 mM NMDA infusion, compared to the decrease of -24±34% with 0.3 mM NMDA infusion. This graded response suggests dentate gyrus (DG) gatekeeping in hippocampus.

In sensorimotor cortex, intracerebral infusion of NMDA at 0.3 mM elicited the predicted increase of glutamate release, with a decrease of qEEG spectral power. . Transcranial PA VSD imaging had -13±37% of fractional neural activity index change during the 20 min of 0.3 mM NMDA infusion, consistent with surround suppression of depolarization as shown by qEEG of motor cortex.

We conclude that transcranial PA VSD imaging distinguished relatively greater cortical inhibition and threshold-level hippocampal focal seizure activity that both correlated with activities reported by qEEG signals. The results show this emerging technology to be an innovative and significant advance of functional neuroimaging.

1. Introduction

Whereas electrophysiological and invasive neurochemical techniques have been valuable in assessing activity within specific neural circuits in brain, there is a distinct need for a noninvasive means to image real-time regional functional activity *in vivo*. In particular, motor cortex and hippocampus are of interest, as they present distinct circuits with clear electrophysiological modulation of excitatory neurotransmission. It is long known that neocortical structures such as the motor cortex exhibit both excitatory and feedforward as well as feedback inhibitory mechanisms driven by NMDA that limit neural activity and modulate oscillatory firing. The focal application of low doses of NMDA is known to activate spreading cortical depression that depends on NMDA receptors (Hansen et al., 1980; Gjedde et al., 1981; Lauritzen et al., 1982; Marrannes et al., 1988). On the other hand, the hippocampal circuit has rows of excitatory pyramidal neurons all aligned in close proximity and similar orientation in the dentate gyrus (DG) with its hyperpolarized resting membrane potential that forms the putative gating for signals from adjacent cortices. Low amplitude excitatory inputs do not depolarize the DG neurons and therefore fail to open the DG gate (Andersen et al., 1966). Low amplitude excitatory signals are insufficient to bring the system to threshold for activation; however, with strong repetitive signals seizure activity can be induced. This is consistent with the hippocampus being the lowest seizure threshold region of the mammalian brain. This all-or-none gating system in the DG is therefore distinct in its circuit dynamics from the motor cortex.

Previous optical imaging approaches to local circuit inhibition (Petersen and Sakmann, 2001; Derdikman et al., 2003; Petersen et al., 2003) applied invasive procedures to overcome superficial imaging depth, and further extension to deeper brain regions such as the hippocampus was prohibitive. The imaging of electrophysiological or neurochemical dynamics within the hippocampus primarily has been accomplished by optical imaging of freshly-sliced brain tissue (Okubo et al., 2010) or magnetic resonance imaging spectroscopy (MRS) for non-invasive quantification of glutamate at high spatial resolution (Crescenzi et al., 2017; Voets et al., 2017). However, optical imaging and MRS suffer from the need to isolate brain tissue *ex vivo* and from slow imaging speed, respectively. The application of two-photon microscopy to measure calcium ion dynamics in specific deep brain structures, including hippocampus, has no temporal resolution in real-time. (Kondo et al., 2017) Therefore, non-invasive, real-time visualization with spatiotemporal resolution would be a significant advance, but such an approach would require neurochemical and electrophysiological characterization to validate the neural activity recorded by EEG.

Photoacoustic (PA) imaging is a hybrid approach combining optics and acoustics that provides a molecular signature to the neural activity assessed by acoustic transcranial imaging (Wang et al., 2003; Wang and Hu, 2012). PA imaging is based on thermo-elastic perturbation of a target evoked by light absorbance from a pulsed laser illumination, which generates radio-frequency (RF) acoustic pressure detected by piezoelectric ultrasound transduction or optical interferometry. With this unique imaging mechanism, several attractive applications have been proposed for preclinical and clinical research with tomographic and microscopic imaging modes, including detection of endogenous contrast of cancer indicators (e.g., melanoma (Zhang et al., 2006), breast microcalcifications (Kang et al., 2014; Kim et al., 2014; Kang et al., 2015)), monitoring of cancer angiogenesis (Yao et al., 2012), oxygen metabolism (Hu, 2016), and quantification of lipid content (Hui et al., 2017; Wu et al., 2017), among others.

Here, we validated *in vivo* transcranial PA neuroimaging of distinct neural circuit mechanisms activated by stimulation of N-methyl-D-aspartate (NMDA) receptors in motor cortex and hippocampus in rat brain *in vivo* through intact skull and scalp. This tri-modal neural sensing approach by means of microdialysis, quantitative electroencephalography (qEEG), and transcranial PA imaging simultaneously monitor neurochemical and electrophysiological changes in neural activity and associated glutamatergic

neurotransmission (Figure 1a). To stimulate these circuits, we infused NMDA by reverse microdialysis that triggered localized changes of extracellular glutamate concentration (Drew et al., 2004) (Young and Bradford, 1991). In the cortex, glutamate and γ- aminobutyric acid (GABA) mediate excitatory and inhibitory synaptic events, respectively. NMDA receptor activation also facilitates the release of neurotransmitter from synaptosomes prepared from terminals in the hippocampus and neocortices (Sherman et al., 1991). We quantified the change of extracellular glutamate concentration evoked by reverse microdialysis by direct microdialysis and high-performance liquid chromatography (HPLC). We combined qEEG with microdialysis to evaluate the effect associated with surround inhibition in the presence of glutamatergic excitation at motor cortex and hippocampus, respectively (Figure 1b). Concurrently, the contrasting electrophysiological results were quantified and confirmed with transcranial PA neuroimaging and qEEG recording (Figure 1c). Each of the three modalities thus provided information with different degrees of specificity, including spatial and temporal specificity from PA imaging, temporal specificity from qEEG, and focal neurochemical specificity from microdialysis in target neural circuits, i.e., motor cortex and hippocampus.

2. Material and Methods

Animal preparation. For the proposed *in vivo* experiments, 8-9-week-old male Sprague Dawley rats (Charles Rivers Laboratory, Inc., MA, United States) weighing 275-390g were used. The use of animals for the proposed experimental protocol was approved by the Institutional Animal Care and Use Committee of Johns Hopkins Medical Institute (RA16M225). Rats were housed in groups of 3 per cage with free access to food and water, and maintained on a 12hr light / 12hr dark cycle.

Fluorescence quenching-based near-infrared voltage-sensitive dye. In the present *in vivo* study, we used the fluorescence quenching-based near-infrared cyanine VSD, IR780 perchlorate (576409, Sigma-Aldrich Co. LLC, MO, United States) as in our previous *in vivo* study differentiating a chemoconvulsant seizure activity (Kang et al., 2017), and it have the analogous chemical structure of PAVSD800-2, our new VSD validated in our previous *in vitro* study.(Zhang et al., 2017) This VSD yields fluorescence emission leading to a reciprocal PA contrast with non-radiative relaxation of absorbed energy.

Microdialysis. On the day of the study the rats were weighed and anesthetized with urethane (1.2mg/kg,). Urethane was given incrementally with alternating ip and sc dosing. Three (3) ml of isotonic saline was given sc on each side of the body to keep the animal hydrated during the experimental procedure. Body temperature was maintained until animal was fully anesthetized and ready for surgery. For PA and EEG studies, an iv catheter was inserted into a tail vein prior to surgery for dye administration during the studies. Once a stable plane of anesthesia was established, hair was shaved from the scalp of each rat for improved optical/acoustic coupling for transcranial PA recording. The rat was placed into a stereotaxic device (Stoeling Co. Wood Dale, IL). This fixation procedure was required to prevent any unpredictable movement during PA or EEG recording of neural activities. A CMA12 microdialysis probe (Harvard Apparatus, Holliston, MA, USA) was implanted into either the right lobe of the frontal cortex (stereotaxic coordinates: 1.5 mm lateral and 3.2 mm anterior to bregma, and 3 mm below the surface of the dura) or the CA_3 region of the right hippocampus (stereotaxic coordinates: 3 mm lateral and 3.8 mm posterior to bregma, and 3.6 mm below the surface of the dura) (Paxinos and Watson, 2014). The probe active exchange surface was 2 × 0.5 mm. For EEG and PA experiments, probes were secured to the skull using dental acrylic cement.

***In vivo* microdialysis**. *In vivo* microdialysis sampling was carried out as previously described (Baumann et al., 2012; Elmore et al., 2017). For infusion experiments, NMDA (Sigma-Aldrich Chemicals, St. Louis,

Mo) was weighed, solubilized, and diluted to the desired concentration in artificial cerebrospinal fluid (NaCl, 147 mmol/L; KCl, 2.7 mmol/L; $CaCl_2$, 1.2 mmol/L; $MgCl_2$, 0.85 mmol/L)(Harvard Apparatus, Holliston, MA, USA) on the study day. Once the probe was inserted and secured, it was perfused with artificial cerebrospinal fluid pumped at a flow rate of 2 μl/min. Samples were collected at 20 min intervals, and immediately transferred to a -80 °C freezer until assayed. To allow sufficient time for the glutamate levels to equilibrate, three baseline samples were collected an hour following initiation of infusion. Following these samples, NMDA was infused into the brain directly through the dialysis probe with the same pump parameters as used for the baseline samples. Dialysate samples were assayed for glutamate by a two-step process using HPLC-ECD on an Eicom HTEC-500 system (EICOM, San Diego, CA, USA). After passing the samples through a separation column, they were processed via a column containing immobilized L-glutamate oxidase enzyme, resulting in the release of hydrogen peroxide. The hydrogen peroxide concentration was then determined using a platinum working electrode. Chromatographic data were acquired online and exported to an Envision software system (EICOM, San Diego, CA, USA) for peak amplification, integration, and analysis.

Quantitative EEG. All EEG recordings utilized a three-electrode paradigm: 1 recording, 1 reference (aligned to the site of activation) and 1 ground over the rostrum. The electrodes (IVES EEG; Model # SWE-L25 – IVES EEG solutions, MA, USA) were fixed with minimal cyanoacrylate adhesive (KrazyGlue), similar to previous protocols (Airan et al., 2017). Data acquisition was performed using Sirenia software (Pinnacle Technologies Inc., Kansas, USA) with synchronous video capture. Data acquisition had a 14-bit resolution, 400Hz sampling rate, and a band pass filter between 0.5 Hz and 60 Hz. The acquisition files were stored in an .EDF format and scored manually, using real time annotations from the experiments. EEG power for 2-second epochs was done using an automated fast Fourier transformation module in Sirenia software (Kang et al., 2018).

Photoacoustic imaging. We used real-time PA data acquisition to record electrophysiological neural activities *in vivo*: an ultrasound research system consisted of an ultrasound linear array transducer (L14-5/38) connected to a real-time data acquisition system (SonixDAQ, Ultrasonix Medical Corp., Canada). The center frequency of the transducer was 7.1 MHz to obtain good sensing depth for neural activities in deep brain tissue. To induce the PA signals, pulsed laser light was generated by a second-harmonic (532 nm) Nd:YAG laser pumping an optical parametric oscillator (OPO) system (Phocus Inline, Opotek Inc., USA), providing 690-900 nm of tunable wavelength range and 20 Hz of the maximum pulse repetition frequency. A bifurcated fiber optic bundle, each 40 mm long and 0.88 mm wide, was used for laser pulse delivery. The PA probe was posed between the outlets of the bifurcated fiber optic bundles using a customized, 3-D printed shell for evenly distributed laser energy density in the lateral direction on rat scalp surface. The alignment of outlets was focused specifically at 20 mm depth. The PA probe was positioned in the sagittal plane to cover the barrel cortex and hippocampus at the same time. Lateral position of the probe was at the contra-lateral side of microdialysis probe: 1.5 mm for motor cortex recording; 3 mm for hippocampus. The distance between the PA probe and the rat skin surface was 20 mm filled with acoustic gel, and the resultant energy density was at ~5 mJ/cm^2 , which is far below the maximum permissible exposure (MPE) of skin to laser radiation by the ANSI safety standards. (Anon, 1975) A wavelength of 790 nm was used, at which sufficient absorbance can be obtained by the near-infrared VSD, i.e., IR780 perchlorate. Also, probing at the wavelength prevented the undesired time-variant change of oxygen saturation, being at the isosbestic point of Hb and HbO_2 absorption spectra. Fig. 4b presents a representative sagittal cross-sectional PA image of a rat brain. The brain outline was drawn based on the rat brain atlas (Paxinos and Watson, 2014). Detailed information of neural activity reconstruction using normalized time-frequency analysis can be found in our previous publication (Kang et al., 2017).

***In vivo* experimental protocol.** The *in vivo* protocols were designed for simultaneous multi-modal sensing of the neural activity at motor cortex and hippocampus: microdialysis-qEEG and microdialysis-PA imaging. Figure 2 shows a detailed schematic protocol for each group representing the response to the administration of NMDA, Lexiscan and VSD (i.e., IR780 perchlorate). PA and qEEG data acquisition was performed for 40 min to correlate with three microdialysis samples collected at 20-min intervals. VSD and Lexiscan followed the data acquisition sequence with 3-min delay, thereby 5 min of baseline phase was guaranteed for neural activity index reconstruction in PA imaging before starting NMDA infusion. The dosing protocol for Lexiscan and VSD administration was as follows: through an iv tail vein catheter, 150 μl of Lexiscan (0.4mg/5ml) was injected, followed by 200 μl of VSD at 2mg/ml concentration, flushed immediately with 150 μl of 0.9% isotonic saline. The EEG signal at motor cortex was recorded an identical preparation procedure as the PA imaging, including animal preparation and administration of IR780, Lexiscan and experimental duration time for all recordings.

Brain histology. Rats used for the above protocol were sacrificed, and whole brains immediately harvested and placed in 10% formalin. All brains were allowed to fix in fresh 10% formalin for at least 48 hours with gentle agitation on a conical rotator. Subsequently, the brains were processed through a series of sucrose gradients (15%, 20%, 30% for 12-24 hours each) for cryoprotection. Brains were sectioned frozen at 300 μm thickness. Tissue sections were mounted on slides in ProLong Diamond Anti-face mountant. Slides with sections were imaged using an Olympus OM-D E-M5 Mark II for bright field image and using LI-COR Odyssey for fluorescence visualization.

3. Results

NMDA-evoked glutamatergic neurotransmission. Intracortical and intrahipocampal infusion of NMDA diluted into artificial cerebrospinal fluid at the required concentrations, was infused through the microdialysis probe. Concentrations of glutamate release in the dialysate were calculated from values of three baseline samples collected at 20 minutes intervals before NMDA infusion. During infusion, samples continued to be collected every 20 minutes for the remainder of the study. Glutamate release were calculated as a % of basal values. Figure 3 shows the effect of NMDA infusion on glutamate release in the motor cortex and the hippocampus of anesthetized rats. Figure 3a shows that infusion of 0.3 mM NMDA into the motor cortex caused a roughly 60 % increase in glutamate levels as compared to baseline samples. The increase occurred in the first 20-minute sample collection period following the onset of NMDA infusion, and was sustained for the full infusion period. Figure 3b demonstrates the dose-related response of NMDA infusion at 0.3, 1.0, and 3.0 mM into the hippocampus, where 0.3 mM NMDA caused a roughly 40% increase in glutamate levels that remained elevated for the duration of the infusion; the 1.0-mM NMDA infusion appears to cause doubling of the glutamate levels in the hippocampus compared to baseline. This increase observed at the 1.0-mM remained elevated through to the end of the NMDA infusion. However, at 3.0-mM, the NMDA infusion raised the glutamate level roughly 6-fold, above baseline level, which peaked during the second 20-minute sampling period, after which it began a steady decline to the termination of the infusion. The increase in glutamate release seen in microdialysis in the motor cortex did not correlates with measures of VSD imaging with PA, but good correlations were seen in the hippocampus. Interestingly, qEEG also revealed no seizure activity with infusion into motor cortex at the 0.3-mM concentration, but elicited a strong seizure response in hippocampus with infusion of 3-mM NMDA in the time period that coincided with peak glutamate activity in the dialysate.

EEG of electrophysiological activity in motor cortex and hippocampus. We used qEEG to investigate whether the NMDA-induced glutamate release seen with microdialysis activates circuits in

motor cortex and hippocampus. In order to establish circuit activity differences of reactivity to the specific focal stimulations, recordings of qEEG were used to interpret PA values acquired with the same protocols to establish spatial and temporal relationship. The temporal specificity of qEEG expressed circuit responses in realtime, before and after focal NMDA infusion. However, qEEG lacks spatial resolution, and records cannot be obtained from deep brain structures with leads placed on brain or skull surfaces. Therefore, we opted not to place in-depth electrodes, in order to maintain the experiments as possible. We made the stimulation focal, according to the previous proof-of-concept results by PA detection onset of generalized seizures through an intact skull (Kang et al., 2017).

When 0.3-3 mM NMDA was delivered to distinct motor cortex and hippocampal circuits by microdialysis probe (Figure 1a) (Paxinos and Watson, 2014), results showed that NMDA infusion of 0.3 mM NMDA at the M2 coordinates of the motor cortex caused the expected rise of local glutamate release measured in microdialysis (Figure 3) that had an effect on qEEG spectral power; specifically in the gamma frequency (Figure 4-a2). The resulting qEEG suppression seem to indicate focal glutamate-induced activation of surround inhibition; becoming more prominent over the duration of the infusion (Figure 4-b2). In contrast, a 3 mM infusion into the hippocampus immediately resulted in increased bursts of gamma power in the EEG, followed by a focal seizure (Figure 4 and S1). Unlike the cortical circuit that showed increasing EEG suppression over time, the hippocampal circuit continued to exhibit short epileptiform discharges throughout the NMDA infusion period (Figure S1b V), indicating continued disruption of the DG gating during the entire duration of the NMDA infusion.

Transcranial PA imaging. Transcranial PA neuroimaging of distinct neural mechanisms in motor cortex and hippocampus was performed at the contralateral position of microdialysis probe (Figure 5a). The PA sagittal planes obtained at 790 nm presented a sufficient sensitivity at the depths of interest in rat forebrain: 2.5 mm and 3.6 mm for motor cortex and hippocampus, respectively (Figure 5b). The motor cortex imaging plane presented high intensity at the superior sagittal sinus at superficial depth, and the morphological boundary of brain tissue could be distinguished based on the rat brain atlas and PA signal distribution representing both blood and VSD in brains. The sagittal PA imaging plane of hippocampus also revealed the cross-sections of transverse sinus and inferior cerebral vein in the superficial depth range, but it also shows sufficient sensitivity at the depth of hippocampus. From the regions-of-interest (ROIs) indicated with solid white box, time-averaged neural activity index was reconstructed pixel-by-pixel for baseline (5 – 10 min) followed by the results for time bins in 10 min interval: 10 – 20 min, 20 – 30 min, and 30 – 40 min (Figure 5c). As a result, the substantial amount of circuit dynamics was detected at hippocampus with 3 mM NMDA infusion, while demonstrating negligible change at motor cortex as predicted by their distinct mechanisms. Otherwise, the hippocampus with 0.3 mM NMDA infusion did not present any significant change, which implies a failure to overcome high activation threshold of DG gatekeeping with 0.3 mM NMDA infusion. This interpretation is supported with the subtle change in extracellular glutamate concentration shown with forward microdialysis (Figure 3b)

To further characterize the PA VSD intensity change, the normalized neural activity index sequence at the ROIs indicated by red dots was plotted as a function of the corresponding normalized PA intensity (Figure 5d). Note that the size of each ROI was 1 x 1 mm^2, and the reference intensity was obtained from the baseline phase: 5-10 min. In motor cortex, 0.3-mM NMDA infusion presented complex suppression mechanism in the cortical region: The quantification of normalized neural activity index presented 1.00 ± 0.36, 0.87 ± 0.37, and 1.19 ± 0.36 for baseline (5 – 10 min), and first (10 – 30 min) and second (30 – 40 min) microdialysis phases (NMDA1 and NMDA2), respectively. This result suggests the initial suppression at the first 20 min of NMDA infusion (i.e., -13 %), which is well correlated to the electrophysiological validation in qEEG recording (Figure 4-a2). On the other hand, 3-mM NMDA infusion at hippocampus yielded significant elevation of neural activity index as corresponding PA intensity decreases: 1.00 ± 0.35 %, 1.55 ± 0.36 %, and 1.74 ± 0.33 % of normalized

neural activity indices for baseline, NMDA1, and NMDA2 phases, respectively. This validates the proposed VSD mechanism which yields suppressive intensity to neuronal depolarization (Zhang et al., 2017). Otherwise, focal 0.3 mM NMDA infusion at hippocampus did not presented any statistically-significant circuit activity increase compared to the baseline neural activity index: 1.00 ± 0.31 %, 0.99 ± 0.41 %, and 0.76 ± 0.34 % of normalized neural activity indices for baseline, NMDA1, and NMDA2 phases, respectively. These results support our hypothesis that PA imaging can differentiate the DG gating function at the hippocampus. In all, when tracing the change of circuit dynamics from the baselines, the 3-mM NMDA infusion at hippocampus presented statistically significant difference compared to those with 0.3 mM at both hippocampus and motor cortex ($P < 0.0001$). The VSD mechanism suppressive to neuronal depolarization could be also confirmed with the temporal specificity of PA neuroimaging. The successful extraction of neural activity index was also confirmed in Figure 5e which presents the normalized neural activity index (top panel) and relative PA intensity to baseband frequency component (bottom panel). As shown in the figure, NMDA inset produces suppressive PA intensity around 1-dB from basal level, which is also synchronized to the focal seizure presented in qEEG given by DG gating breakdown (Figure 4-b2 and Figure S1 V), leading to 2.5-times instantaneous increase of neural activity index for around 20 sec. Refer Figure S2 for the entire neural activity index and PA intensity traces.

Figure 6 presents the normalized neural activity index as a function of extracellular glutamate concentration at motor cortex and hippocampus. The motor cortex presents the comparable amount of neural activity index with that of baseline phase at hippocampus (n = 1), but 3 mM NMDA infusion into hippocampus produced exponential increase in neural activity index when the extracellular glutamate concentration exceeds 6 μM in microdialysis sampling (n = 2). These results again confirm the DG breakdown with specific glutamatergic potential threshold at neural circuitry.

Brain histology. Brain tissue was extracted after all *in vivo* experimental protocols. The brain was frozen-sectioned *into* 300-μm thickness slices and evaluated to confirm probe placement using the hemorrhage caused by the microdialysis probe insertion for the NMDA infusion and collections as a marker. Figure 6 shows the bright-field images of the coronal plane of the motor cortex and hippocampus at 3.2 mm and -3.8 mm from bregma, respectively. White arrows indicate the hemorrhage caused by the microdialysis probe positioned at the following coordinates: bregma 3.2 mm, lateral 1.5 mm, depth 2.5 mm for motor cortex; bregma -3.8 mm, lateral 3 mm, and depth 3.6 mm for hippocampus. The VSD staining of brain tissue was confirmed with near-infrared fluorescence microscopy. Uniform VSD fluorescence was found in the VSD perfusion group, while negative control (VSD -) presented negligible fluorescence emission (Figure S3), which confirms the results in our previous publication (Kang et al., 2017).

4. Discussion

The application of PA imaging was expanded to neuroscience (Nie et al., 2012; Liu et al., 2017; Li et al., 2018) as label-free transcranial PA imaging of neurovascular coupling proposed as a means to quantify hemodynamic changes (Hu and Wang, 2010; Zhang et al., 2018). However, this approach does not yield quantitative neural activities that directly correspond to electrical activity, as required for the proposed imaging of distinct neural mechanisms within motor cortex and hippocampus. Hemoglobin provides an effective contrast signal, and there has been extensive investigations into more effective exogenous contrast agents (Luke et al., 2011; Huynh et al., 2014; Moon et al., 2015; Ju et al., 2016; Weber et al., 2016). Several PA approaches detect electrophysiological neural activities with functional voltage sensors. Deán-Ben et al. showed real-time PA tomography of a genetically encoded calcium indicator, GCaMP5G, using zebrafish *in vivo* (Deán-Ben et al., 2016). Sheryl Roberts, et al. also proposed a new

metallochromic calcium sensor for PA imaging (CaSPA) which has a high extinction coefficient, a low quantum yield, and high photo-bleaching resistance for brain and heart imaging (Roberts et al., 2018). Ruo et al. reported PA imaging of neural activity evoked by electrical stimulation and 4-aminopyridine-induced epileptic seizures using hydrophobic anions such as dipicrylamine (DPA) in mouse brain.(Rao et al., 2017) However, these voltage sensors requires PA imaging at the visible spectral range (488 nm and 530 nm for GCaMP5G; 550 nm for CaSPA; 500 nm and 570 nm for DPA), which is suboptimal for the proposed study when especially imaging hippocampus posed at 5 mm – 8 mm including intact scalp and cortex for the rat (Nowak et al., 2011; Paxinos and Watson, 2014). Recently, we proposed transcranial PA recordings of brain activity *in vivo* with a near-infrared voltage-sensitive dye (VSD, 790 nm), delivered through the blood-brain barrier (BBB) via pharmacological modulation, as a promising tool to transcend current functional neuroimaging limitations, particularly as it relates to sensing depth (Kang et al., 2017; Zhang et al., 2017). The studies demonstrated that transcranial PA imaging of near-infrared VSD distinguishes *in vivo* seizure activity in stimulated rat brains from that of control groups in real time (Kang et al., 2017). However, the results were limited by the use of a global chemoconvulsant, causing perturbation across the entire brain caused by the intraperitoneal administration of penetylenetetrazole (PTZ). In this paper, we presents further advances in PA VSD imaging focal neural stimulation of heterogeneous neural circuits, with concomitant validations from qEEG and glutamate quantification using microdialysis, respectively.

The set of experiments described here yield key findings as follows: (1) The microdialysis-dependent NMDA infusion into the central nervous system (CNS) lead to a reliable increase in focal extracellular glutamate concentrations in both the cortex and hippocampus. (2) Unlike the microdialysis glutamate release for both cortex and hippocampus, transcranial PA imaging and qEEG showed distinct phenotypes in the cortex vs. hippocampus. There was a fall in electrophysiological responses in the motor cortex indicating NMDA receptor activation in the motor cortex circuit lead to strong activation of local inhibitory circuits either directly or as a consequence of activation of feedback circuits (Sachdev et al., 2012). In contrast, NMDA activation in the hippocampus triggers an all-or-none type of circuit dynamics that lead to the initiation of a focal seizure in the hippocampal circuit. (3) Transcranial PA neuroimaging data successfully validated these EEG specific opposite circuit activity profiles for the similar focal activation of NMDA receptors. No circuit activity was detected in the motor cortex on the PA imaging despite an increase in focal glutamate levels recorded in the same rats. In contrast, the PA signal yielded hot spots of neuronal activity following NMDA receptor activation in the hippocampus.

These results allow us to reassess the differential neural mechanisms modulating activity between motor cortex and hippocampus as described in the Introduction: Strong local circuit inhibition has been observed with transcranial PA neuroimaging and qEEG recording. Cortical inhibition may be due to suppression of neuronal firing mediated by γ-amino butyric acid (GABA) receptors (Krnjević, 1997) secondary to activation of GABAergic inhibitory interneurons by NMDA (Homayoun and Moghaddam, 2007). Slice electrophysiology in animal and human cortical tissue have revealed two main phases of inhibition following stimulation; a "fast" phase mediated by ionotropic $GABA_A$ receptors and a "slow" phase mediated by metabotropic $GABA_B$ receptors (Connors et al., 1988; McCormick, 1989). Inhibition provides the ability to locally modulate excitation as well as gate rhythmic activity, which is critical for proper sensorimotor inputs and outputs. Such findings likely indicate a general pattern of cellular connectivity intrinsic to cortical organization.

On the other hand, the hippocampal circuitry provides a second distinct circuit that contrasts with that of the motor cortex to assess PA specificity, as it reveals the proportional excitation of glutamatergic neurotransmission. The DG of the hippocampus is positioned as a gatekeeper for the canonical trisynaptic circuit, regulating the vast cortical inputs that regulate the limbic system. Characteristically, the DG displays a high activation threshold; a trait that is associated with executing

cognitive functions that require pattern separation and completion (Chawla et al., 2005). The ability to differentiate inputs, and diversify cognitive functions, is mediated by inhibition. Suitably, the DG is profusely innervated with strong GABAergic inhibition (Szabo et al., 2017). In diseases of hyperexcitability, such as epilepsy, the DG can regulate pathological seizure activity from invading the limbic system. This gating is evident in recordings from the DG during low frequency stimulation of the perforant path fibers. The DG displays the ability to selectively filter low frequency stimulation by subsequent activation of strong inhibitory post synaptic potentials (Andersen et al., 1966). Yet, longer or higher frequency stimulations resulted in excitatory post synaptic potentials generated by the DG. This disruption of DG gating has been clearly demonstrated by utilizing VSD imaging techniques, reinforcing DG's role of gatekeeping (Ang et al., 2006). The consequence of gatekeeping is that in epilepsy the DG generates and propagates seizure activity.

Further investigations are required to advance our current perspectives available with tri-modal sensing, including PA, qEEG, and microdialysis. Previous studies have shown that application of glutamate to the hippocampal pyramidal neurons produces a fast-rising brief depolarization (Taube and Schwartzkroin, 1987). Therefore, the use of PA will enable us to more precisely assess glutamate and GABA dynamics in order to formulate a more complete profile of circuit activation. Once homeostasis is disrupted, neuronal activity is sensitive to changes both of excitatory and inhibitory mechanisms. . Faster neurochemical recording is another approach that may prove useful in assessing the impact of these measures. Although microdialysis successfully provided quantitative, focal neurochemical concentrations, the sampling rate of 1 sample per 20 min was slow. Techniques offering faster temporal resolution may allow more meaningful comparison of the neurochemical changes yielded by microdialysis and the electrophysiological events monitored by qEEG and PA imaging. One such technique, using custom built hardware and the Amplex Red method, achieved fluorescence-based quantification of glutamate from samples taken every 5 seconds, though reliability appeared to be limited when higher glutamate concentrations were measured (Medina-Ceja et al., 2015). Implantable glutamate biosensors allow sub-second readouts of neurochemical concentrations. However, current limitations include sensitivity, selectivity, and high cost; recent developments in materials, effective modeling, and sensor design may soon alleviate some of these limitations (Clay and Monbouquette, 2018; Moon et al., 2018).

EEG records the voltage differentials occurring between the reference and recording electrode representing underlying circuit activity with high temporal specificity. Hypersynchronous neuronal activity in any given circuit results in high amplitude high frequency activity in the EEG, causing the generation of potent local excitatory events. In contrast, interneurons known to fire action potentials at very high frequencies inhibit neuronal circuit activity efficiently because a single interneuron can innervate and inhibit a large population of pyramidal neurons simultaneously. Depending on the circuit, simultaneous interneuron activation can be followed by a rebound depolarization due to simultaneous disinhibition of the excitatory neurons innervated by this interneuron population.

Based on the validated circuit activity measured via transcranial PA imaging and qEEG successfully differentiated the circuit activity between these regions with spatial and temporal specificity. However, future developments should serve to further advance the efficacy of PA imaging in neuroscience. (1) We expect that improved signal processing for extracting neural activity from the ubiquitous blood context will enable better characterization of brain function. The present in vivo experiments confirmed the possibility of background suppression. Enhanced signal processing and/or use of multi-spectral wavelengths may allow significantly improved spectral differentiation of electrophysiological activities in the brain, leading to development of novel quantitative metrics for real-time brain activity measures. Having isotropic resolution with 2-D PA probe would be also an interesting direction to pursue as follow up to the present work. The use of 2-D PA probe would not only allow

real-time volumetric information, but also enable the suppression of off-axis interference. Even though we presented that neural activity can be successfully discerned with current 1-D PA probe, its sensitivity might be affected by off-axis interferences especially from the elevation direction because of the limited acoustic lens focusing at a fixed depth. The neuroimaging using 2-D PA probe would reject those interferences by the advanced electrical beamforming capability in axial, lateral, and elevation directions.

In all, the EEG results indicate that NMDA infusion and the associated increase in focal glutamate had opposite physiological results in the two circuits: NMDA triggers glutamate release that excites the neural circuit, but it is nearly immediately blocked by surround inhibition at motor cortex or causes runaway excitation in the hippocampus by overcoming DG gating. This is reflected in the lower seizure threshold of the hippocampus compared to neocortex. This suggests that the activations of NMDA receptors can modulate neural circuits into diametrically opposite responses *in vivo*. Transcranial PA imaging demonstrated its ability to differentiate the changes in electrophysiology found in these circuits, and its findings were validated with qEEG. PA imaging is a promising technology for the imaging of neural events in real time.

Author Contributions

DFW , AAG and MB originally conceived of the NMDA administration and of microdialysis with PA idea and helped to design the overall research plan . DFW critically revised the focus of the results and final version and interpretation. LML SDK, helped to design the overall research plan, helped plan specific experiments and all contributed to the review and writing of the manuscript. Jeeun K, SDK, JSE, BJS, HV planned and carried out *in vivo experiments*, analysed the research outcomes, and wrote key elements of the first draft of the manuscript. Jeeun K analysed and interpreted with EB the PA measurements, HV and JE the NMDA dosing design and microdialysis and SDK and BS the EEG experiments HV and LML devised the VSD vehicle preparation. APM performed histopathological analysis. - MH planned and supervised confirmation of VSD penetration into brain tissue also contributed to the final version of the manuscript. AG critically revised experimental design, draft, and final versions of manuscript, and interpretation of results. Jin K developed, funded, and participated in the current PA system design. AR participated in early planning and critically read and edited the manuscript. He has contributed both technically and materially to support this research. EB led the development, system specification, design specification, and funding of the current photoacoustic system. Secured the funding of the needed imaging experiments throughout the life time of the project, including taking responsibility of 3 full-time research members specifically for this work, JK and AM. Further, he has contributed intellectually by mentoring these members and providing input on manuscripts, and participating on PI meetings. DFW, AR and AG provided the original funding for the in vivo experiments MB provided resources and personnel and vital collaboration for the microdialysis part of the experiment.

1 Funding

This work was supported by the NIH Brain Initiative under Grant No. R24 MH106083-03 (DFW, AR, AG, EB AG HV, JE) and the NIH National Institute of Biomedical Imaging and Bioengineering under Grant No. R01EB01963. NIH National Institute of Child Health and Human Development (NICHD) for R01HD090884 (SDK). NIH National Institute of Heart, Lung and Blood (NHLBI) under grant number R01HL139543. National Cancer Institute (NCI) under grant number R21CA202199 and its equipment supplement. Funding of the PA equipment via resources of Jin K and EB NSF Career award #1653322

2 Conflict of Interest Statement

The authors declare that the research was conducted in the absence of any commercial or financial relationships that could be construed as a potential conflict of interest.

481 **Figures**

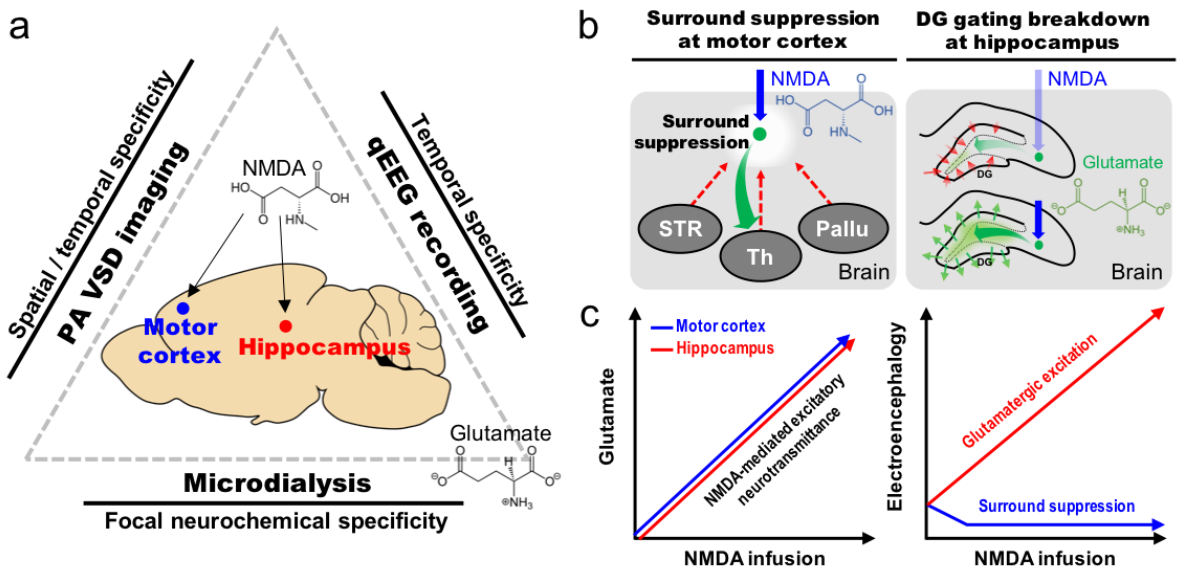

482

483 **Figure 1 Tri-modal sensing of distinct changes in electrophysiology at motor cortex and hippocampus.**
484 (**a**) Tri-modal neural sensing approach. (**b**) Surround suppression at motor cortex and dentate gyrus (DG) gating
485 breakdown at hippocampus to a focal NMDA infusion. (**c**) Diversion of an electroencephalogy for NMDA-
486 mediated glutamatergic neurotransmissions. NMDA, N-methyl-d-aspartate; STR, subthalamic nucleus; Th,
487 Thalamus; Pallu, Pallidus.

488

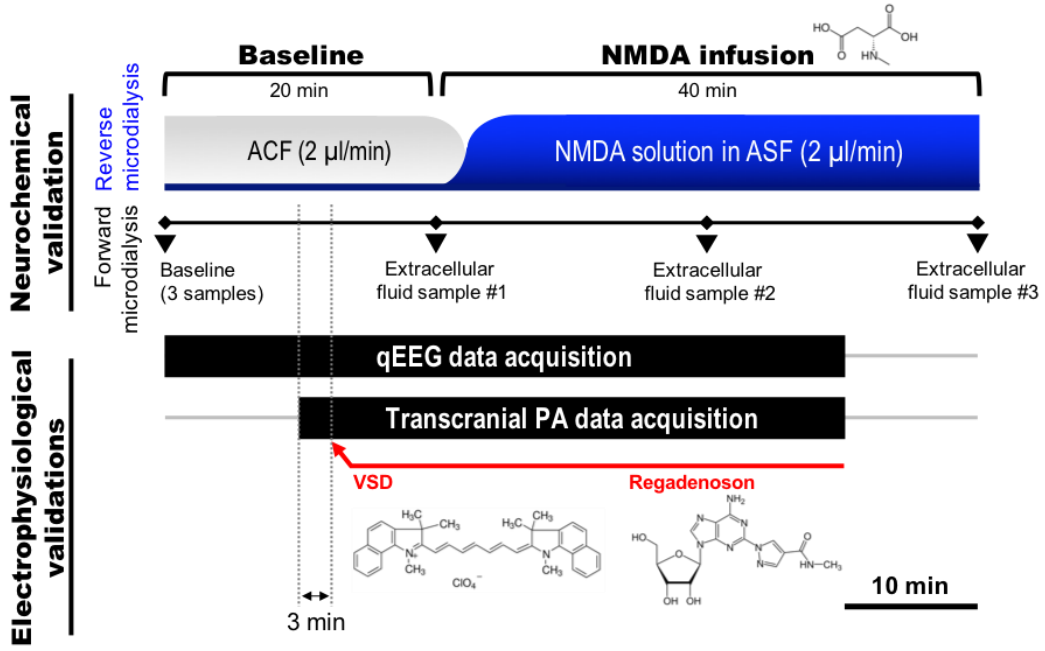

489

490 **Figure 2 *In vivo* experimental protocol.** Tri-modal sensing of distinct mechanisms at motor cortex and
491 hippocampus using forward microdialysis, PA imaging, and qEEG. ACF, artificial cerebrospinal fluid.

492

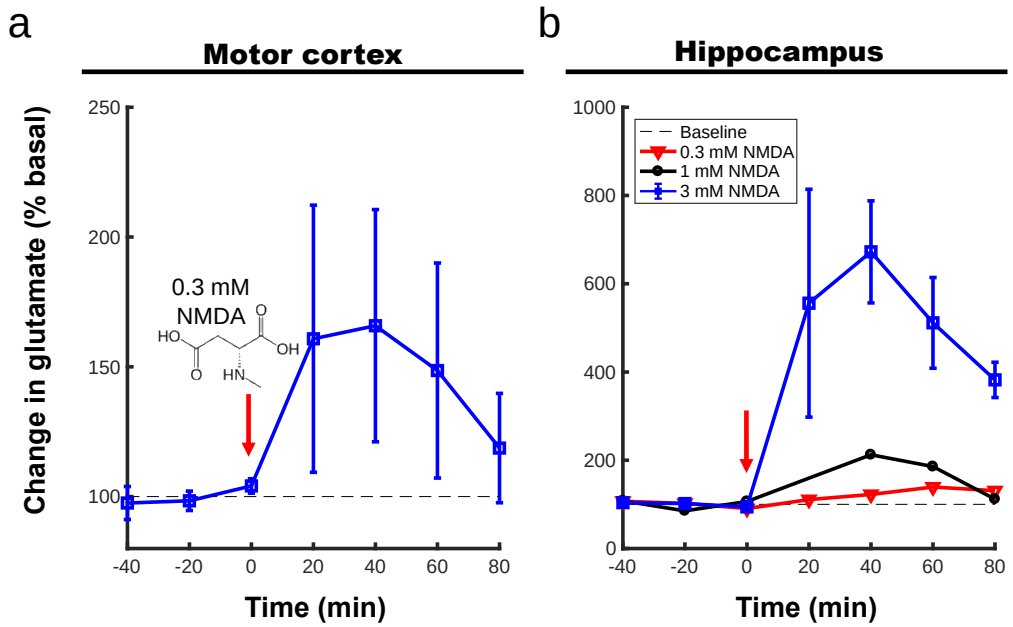

Figure 3. The effects of NMDA infusion on extraceullular glutamate concentrations in anesthetized rats, as compared to % baseline. (**a**) 0.3 mM NMDA infusion into the motor cortex causes the glutamate to increase, culminating in a 65% increase as compared to % baseline. (**b**) 0.3, 1.0, and 3.0 mM NMDA infusion into the hippocampus caused maximal glutamate increases of 39%, 112%, and 572% respectively as compared to % baseline.

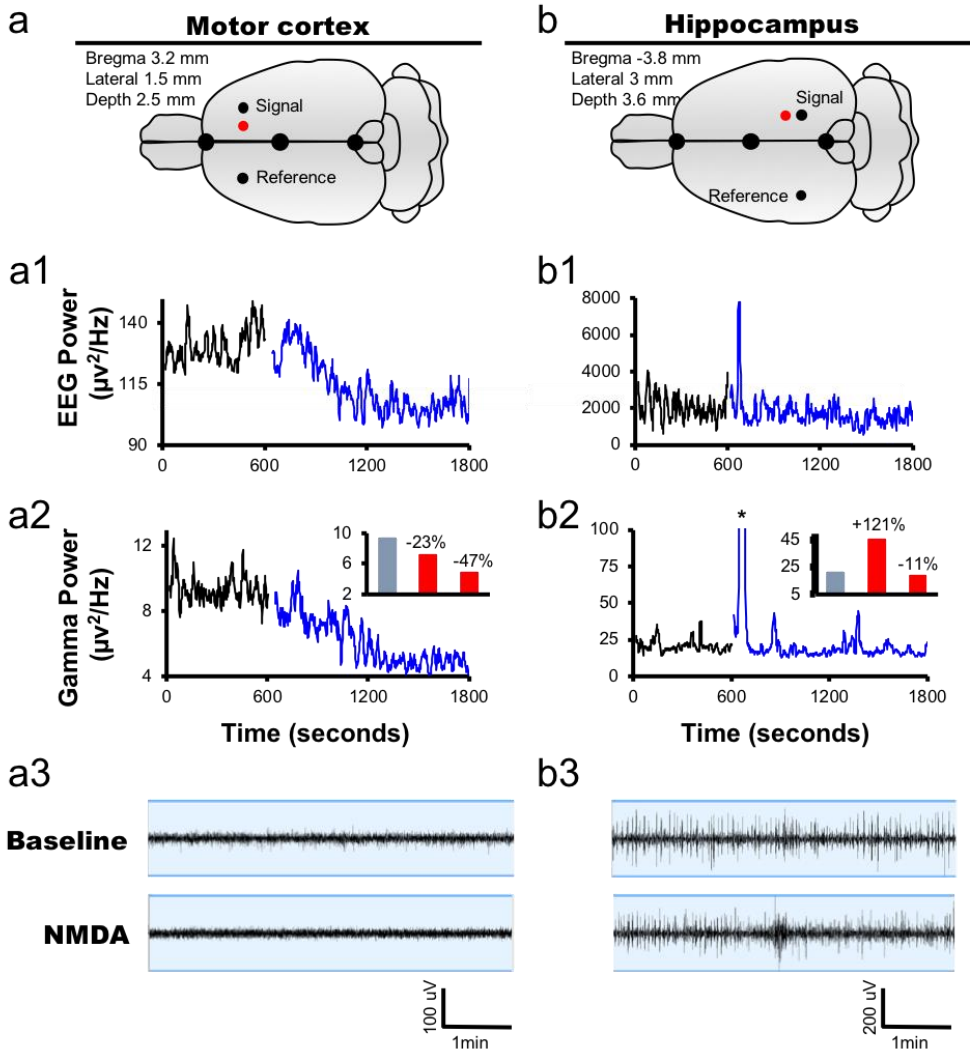

Figure 4. qEEG of motor cortex and hippocampus circuit dynamics following focal NMDA infusion. (**a**) Illustrates stereotaxic coordinates for the microdialysis probe and recording leads for the motor cortex. Ground electrode was implanted over the rostrum for both locations. Full EEG power (**a1**) shows a 10-minute baseline recording (blue trace), followed by two consecutive 10 min traces (red traces) of focal NMDA infusion. Overall EEG showed a drop in power after onset of focal NMDA infusion. (**a2**) Respective gamma power with baseline (blue trace) and focal NMDA infusion (red trace); power drop in gamma over the NMDA infusion period (first 10-minutes 23% decrease, second 10-minute 47% decrease when compared to baseline; see inset). (**a3**) Five minute raw EEG traces, blue lines indicate +/- 200uV, (attenuation of EEG waveforms seen with NMDA). (**b**) Illustrates stereotaxic coordinates for the microdialysis probe and recording leads for the hippocampus. Full EEG power (**b1**) shows a 10-minute baseline recording (blue trace), followed by two consecutive 10 min traces (red) of focal NMDA infusion. In contrast to the motor cortex, hippocampal EEG demonstrated onset of epileptiform discharges. (**b2**) Respective gamma power trace for hippocampal recordings demonstrates a 121% increase in gamma in the first ten minutes, and an 11% decrease in the second ten minutes, when compared to baseline (see inset). (**b3**) Five-minute raw EEG traces of the hippocampus, blue lines indicate +/- 200uV, NMDA infusion increased epileptiform activity, seizure indicated by asterisk in b2. For expanded time scales of hippocampal seizure see Supplemental 1.

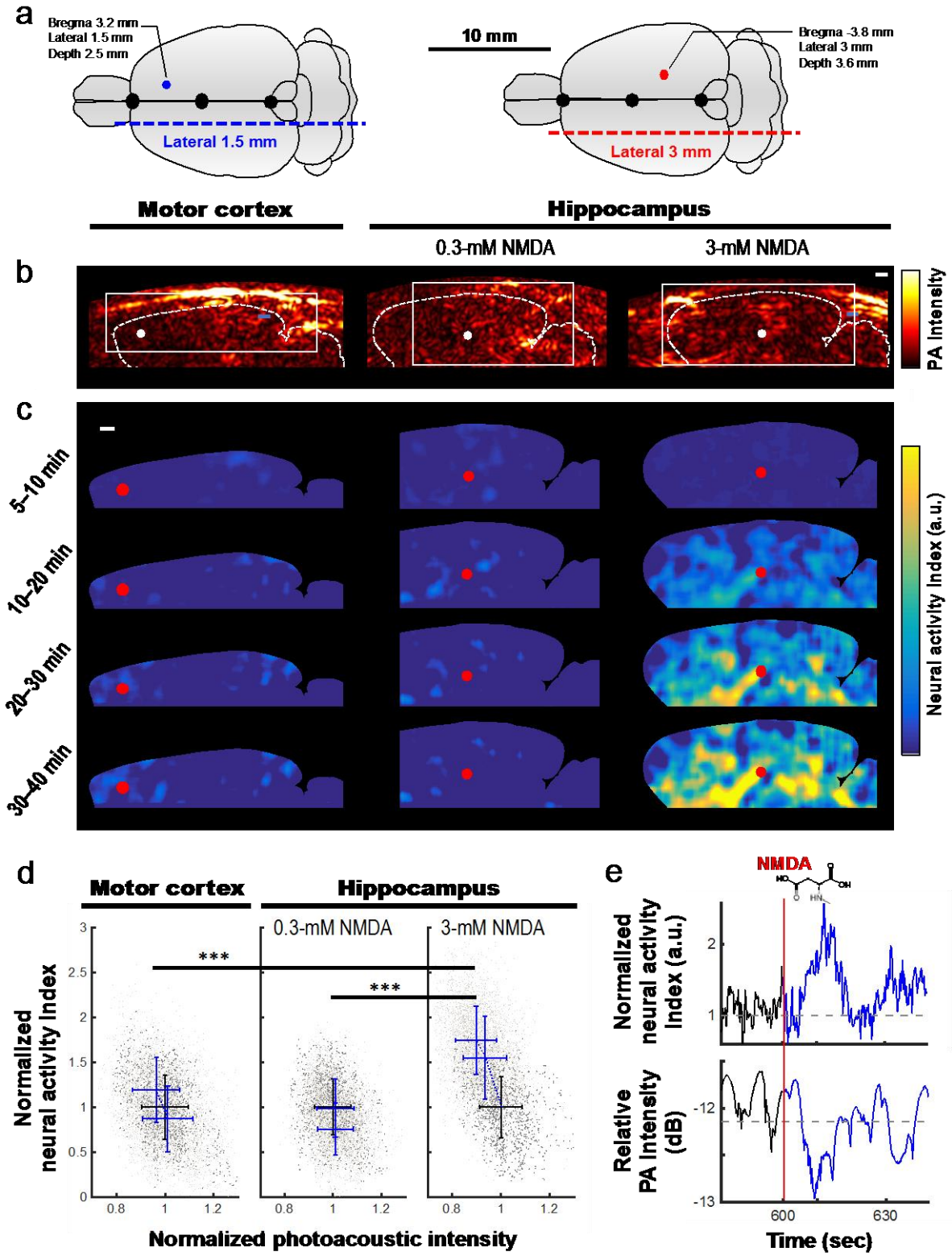

Figure 5. Transcranial PA neuroimaging of the distinct circuit dynamics at motor cortex and hippocampus following focal NMDA infusion. (**a**) Illustration of stereotaxic coordinates for the microdialysis probe and sagittal cross-sections for real-time PA recording. The sagittal PA imaging plane was selected in the contralateral side of the microdialysis probe infusing NMDA into the brain – motor cortex and hippocampus were recorded at 1.5 mm and 3 mm of lateral positions, respectively. (**b**) Sagittal

PA cross-sections at 790 nm and (**c**) time-averaged neural activity maps at each time points: 5-10 min; 10-20 min; 20-30 min; 30-40 min. Note that the points in (**b**) and (**c**) indicate microdialysis probe in contra-lateral positions. Dotted line indicates the boundary of sagittal section derived from the rat brain atlas and scaled accordingly (Paxinos and Watson, 2014), and dotted rectangular indicators are the regions for temporal-frequency analysis reconstruction. (**d**) Normalized neural activity indices as a function of corresponding normalized PA intensities. Black lines: baseline; blue lines: first and second NMDA infusion phases. Dotted blue line indicates the progression of the correlation between the normalized neural activity indices and PA intensities. Gray dots in the background represent the distributions of individual data points: bold gray, data points in baseline; light gray, data points with NMDA infusion. (**e**) Instantaneous suppression of PA intensity at the onset of NMDA infusion, which also presented with qEEG in Figure 4-b2, leading to the high-intensity neural activity index trace. Gray dotted lines indicate the basal level measured during baseline phase, i.e., 5 – 10 min.

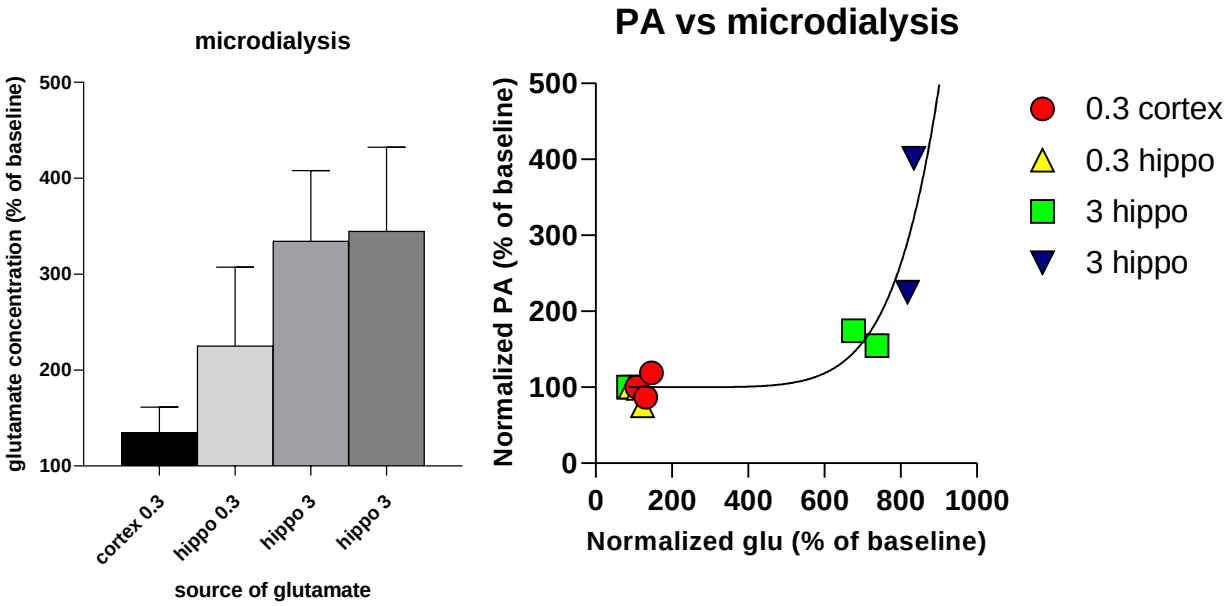

Figure 6. Normalized neural activity index (right panel) as a function of extracellular glutamate concentration (left panel) at motor cortex and hippocampus.

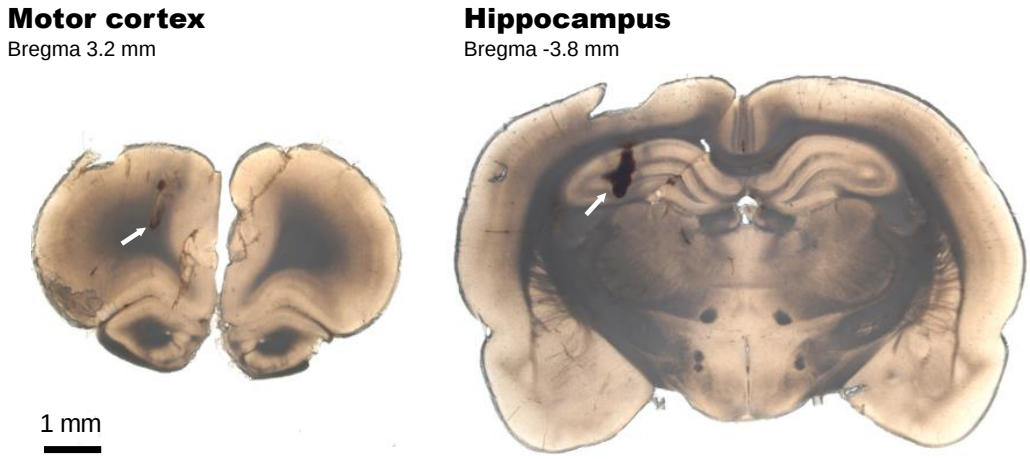

Figure 7. Histopathological confirmation of microdialysis probe at motor cortex and hippocampus. White arrow indicates the wound caused by microdialysis probe installation.

Supplementary Material

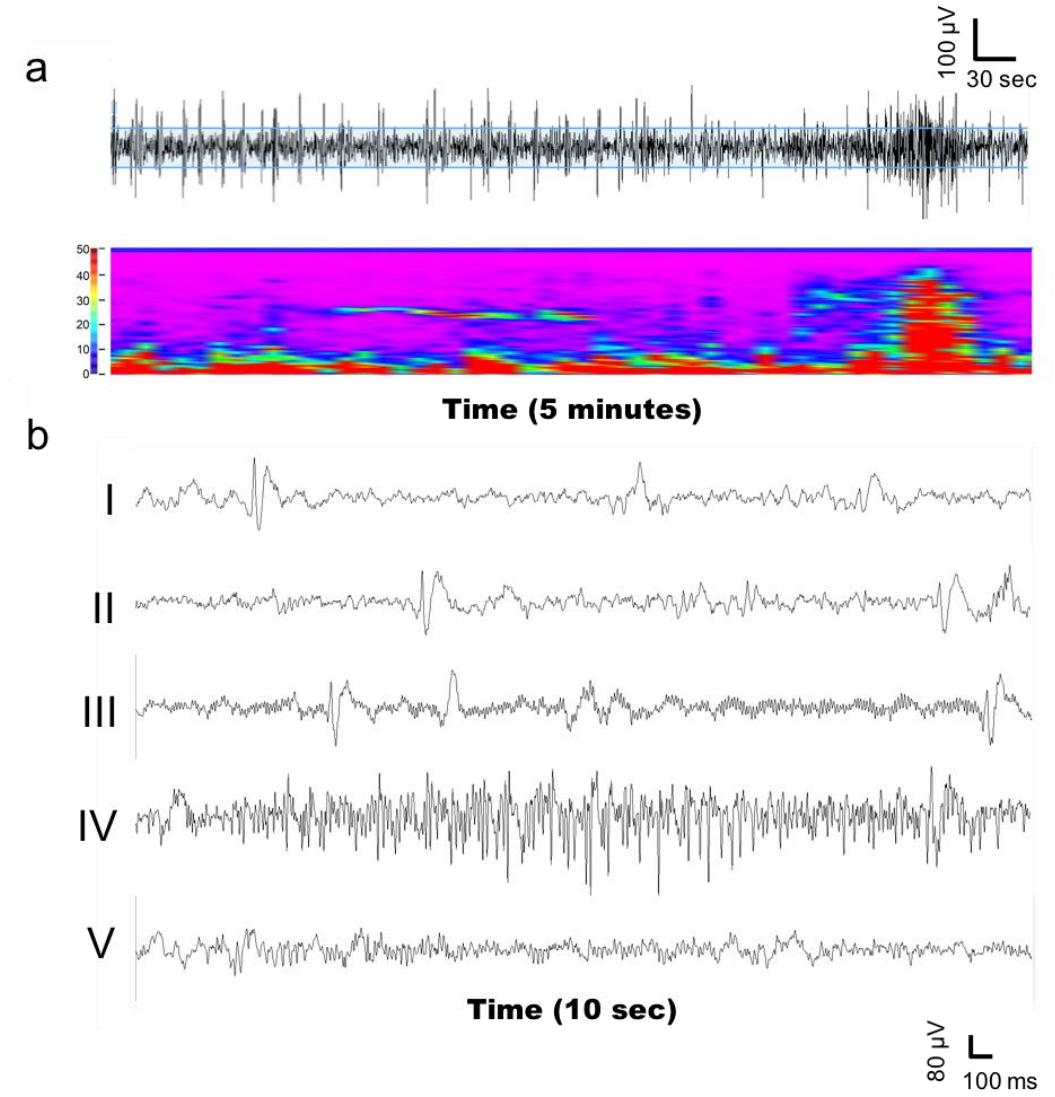

Figure S1. Expanded time scale of EEG recording in the hippocampus. (**a**) Raw trace (5 minutes) shows ramping up of gamma power (see heatmap, 0-50Hz) before onset of focal seizure. (**b**) 10 second expanded time scale of raw EEG traces from hippocampal EEG recording. (I) Baseline (II) immediately after onset of NMDA infusion (III) ramping up of gamma power before seizure event (IV) focal seizure event (V) short duration high frequency hippocampal discharges over the duration of the 20 minute recording (n=1).

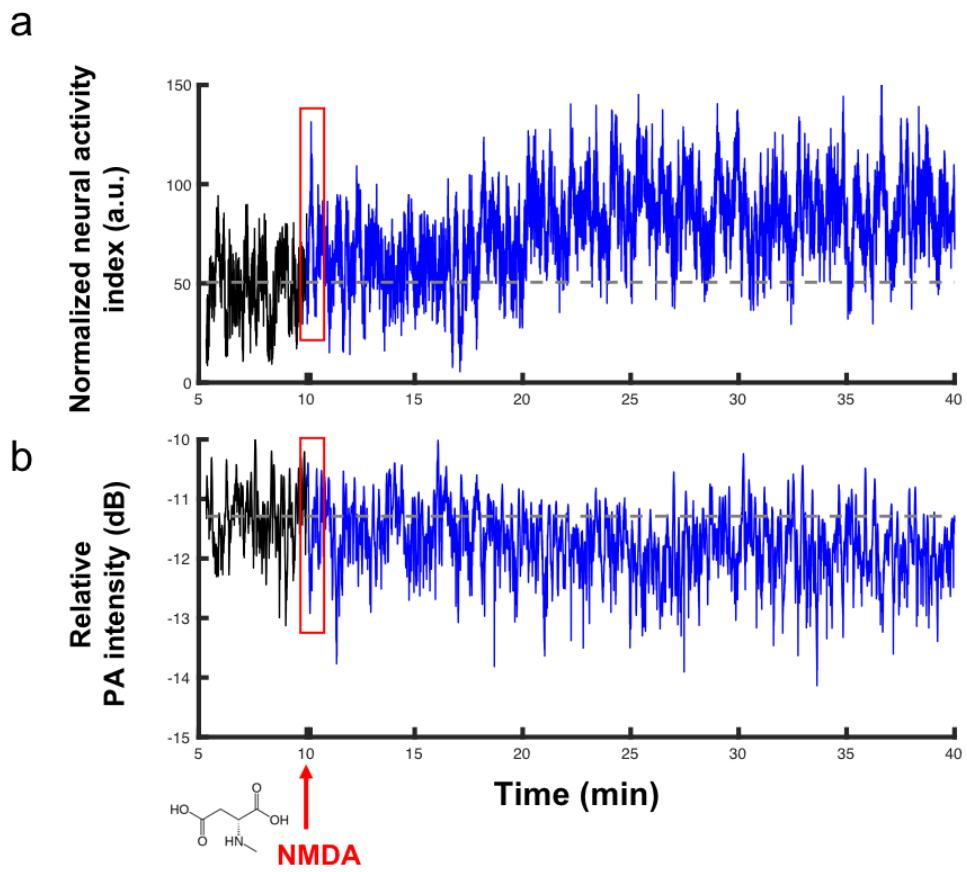

Figure S2. PA quantification of a focal seizure with 3 mM NMDA infusion at hippocampus. (**a**) normalized neural activity index and (**b**) corresponding relative PA intensity traces. Red rectangular indicators show the regions-of-interest used for Figure 5d. Gray dotted lines indicate the basal level measured in baseline phase: 5 – 10 min.

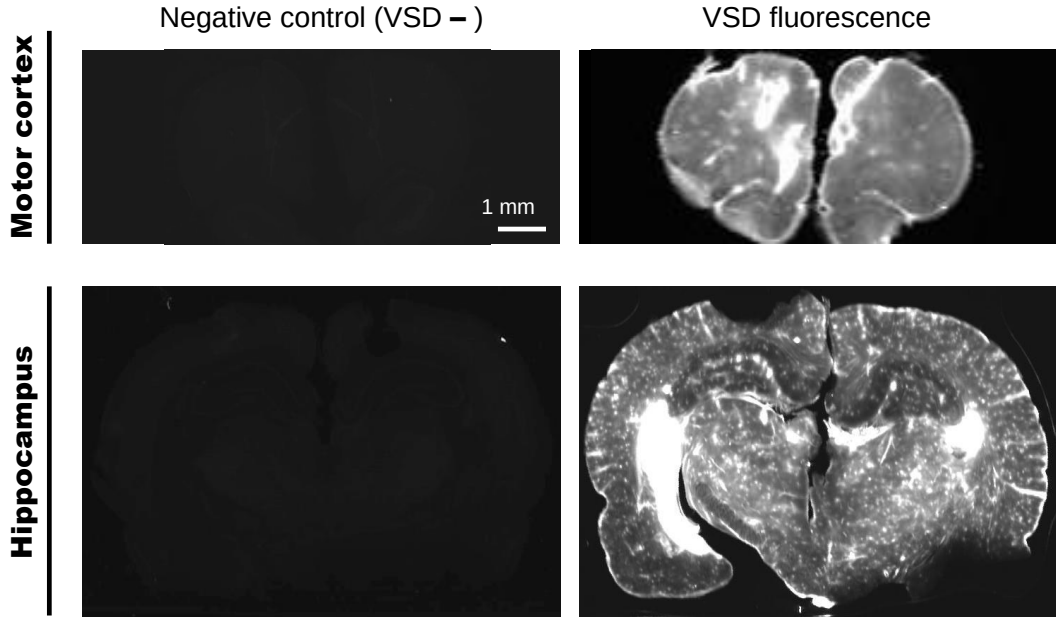

Figure S3. Frozen-sectioning histopathological confirmation of systematic VSD delivery through BBB using pharmacological modulation.

564 **References**

565 Airan RD, Meyer RA, Ellens NPK, Rhodes KR, Farahani K, Pomper MG, Kadam SD, Green JJ (2017)
566 Noninvasive Targeted Transcranial Neuromodulation via Focused Ultrasound Gated Drug Release
567 from Nanoemulsions. Nano Lett 17:652–659.

568 Andersen P, Holmqvist B, Voorhoeve PE (1966) Entorhinal Activation of Dentate Granule Cells. Acta
569 Physiologica Scandinavica 66:448–460.

570 Ang CW, Carlson GC, Coulter DA (2006) Massive and specific dysregulation of direct cortical input to
571 the hippocampus in temporal lobe epilepsy. J Neurosci 26:11850–11856.

572 Anon (1975) American National Standard for the Safe Use of Lasers. Annals of Internal Medicine
573 82:132.

574 Baumann MH, Ayestas MA, Partilla JS, Sink JR, Shulgin AT, Daley PF, Brandt SD, Rothman RB, Ruoho
575 AE, Cozzi NV (2012) The designer methcathinone analogs, mephedrone and methylone, are
576 substrates for monoamine transporters in brain tissue. Neuropsychopharmacology 37:1192–1203.

577 Chawla MK, Guzowski JF, Ramirez-Amaya V, Lipa P, Hoffman KL, Marriott LK, Worley PF,
578 McNaughton BL, Barnes CA (2005) Sparse, environmentally selective expression of Arc RNA in the
579 upper blade of the rodent fascia dentata by brief spatial experience. Hippocampus 15:579–586.

580 Clay M, Monbouquette HG (2018) A Detailed Model of Electroenzymatic Glutamate Biosensors to Aid
581 in Sensor Optimization and in Applications in Vivo. ACS Chem Neurosci 9:241–251.

582 Connors BW, Malenka RC, Silva LR (1988) Two inhibitory postsynaptic potentials, and GABAA and
583 GABAB receptor-mediated responses in neocortex of rat and cat. The Journal of Physiology
584 406:443–468.

585 Crescenzi R, DeBrosse C, Nanga RPR, Byrne MD, Krishnamoorthy G, D'Aquilla K, Nath H, Morales
586 KH, Iba M, Hariharan H, Lee VMY, Detre JA, Reddy R (2017) Longitudinal imaging reveals
587 subhippocampal dynamics in glutamate levels associated with histopathologic events in a mouse
588 model of tauopathy and healthy mice. Hippocampus 27:285–302.

589 Deán-Ben XL, Sela G, Lauri A, Kneipp M, Ntziachristos V, Westmeyer GG, Shoham S, Razansky D
590 (2016) Functional optoacoustic neuro-tomography for scalable whole-brain monitoring of calcium
591 indicators. Light Sci Appl 5:e16201–e16207.

592 Derdikman D, Hildesheim R, Ahissar E, Arieli A, Grinvald A (2003) Imaging spatiotemporal dynamics
593 of surround inhibition in the barrels somatosensory cortex. J Neurosci 23:3100–3105.

594 Drew KL, Pehek EA, Rasley BT, Ma YL, Green TK (2004) Sampling glutamate and GABA with
595 microdialysis: suggestions on how to get the dialysis membrane closer to the synapse. J Neurosci
596 Methods 140:127–131.

597 Elmore JS, Dillon-Carter O, Partilla JS, Ellefsen KN, Concheiro M, Suzuki M, Rice KC, Huestis MA,
598 Baumann MH (2017) Pharmacokinetic Profiles and Pharmacodynamic Effects for Methylone and Its
599 Metabolites in Rats. Neuropsychopharmacology 42:649–660.

600

Gjedde A, Hansen AJ, Quistorff B. Blood-brain glucose transfer in spreading depression. J Neurochem. 1981 Oct; 37(4):807-12. PubMed PMID: 7320723

Hansen AJ, Quistorff B, Gjedde A. Relationship between local changes in cortical blood flow and extracellular K+ during spreading depression. Acta Physiol Scand. 1980 May; 109(1):1-6. PubMed PMID: 7446156.

Homayoun H, Moghaddam B (2007) NMDA receptor hypofunction produces opposite effects on prefrontal cortex interneurons and pyramidal neurons. J Neurosci 27:11496–11500.

Hu S (2016) Listening to the Brain with Photoacoustics. IEEE J Select Topics Quantum Electron 22:117–126.

Hu S, Wang LV (2010) Neurovascular photoacoustic tomography. Front Neuroenergetics 2:10.

Hui J, Cao Y, Zhang Y, Kole A, Wang P, Yu G, Eakins G, Sturek M, Chen W, Cheng J-X (2017) Real-time intravascular photoacoustic-ultrasound imaging of lipid-laden plaque in human coronary artery at 16 frames per second. Sci Rep 7:1417.

Huynh E, Jin CS, Wilson BC, Zheng G (2014) Aggregate enhanced trimodal porphyrin shell microbubbles for ultrasound, photoacoustic, and fluorescence imaging. Bioconjugate Chem 25:796–801.

Ju K-Y, Kang J, Pyo J, Lim J, Chang JH, Lee J-K (2016) pH-Induced aggregated melanin nanoparticles for photoacoustic signal amplification. Nanoscale 8:14448–14456.

Kang J, Chung WY, Kang S-W, Kwon HJ, Yoo J, Kim E-K, Chang JH, Song T-K, Lee S, Kwak JY (2014) Ex Vivo Estimation of Photoacoustic Imaging for Detecting Thyroid Microcalcifications Chen X, ed. PLoS ONE 9.

Kang J, Kim E-K, Kim GR, Yoon C, Song T-K, Chang JH (2015) Photoacoustic imaging of breast microcalcifications: a validation study with 3-dimensional ex vivo data and spectrophotometric measurement. J Biophoton 8:71–80.

Kang J, Zhang HK, Kadam SD, Fedorko J, Valentine H, Kang JU, Rahmim A, Gjedde A, Loew LM, Wong DF, Boctor EM (2017) Transcranial real-time *in vivo* recording of electrophysiological neural activity in the rodent brain with near-infrared photoacoustic voltage-sensitive dye imaging. BioRxiv: 1–23.

Kang SK, Ammanuel S, Thodupunuri S, Adler DA, Johnston MV, Kadam SD (2018) Sleep dysfunction following neonatal ischemic seizures are differential by neonatal age of insult as determined by qEEG in a mouse model. Neurobiol Dis 116:1–12.

Kim GR, Kang J, Kwak JY, Chang JH, Kim SI, Youk JH, Moon HJ, Kim MJ, Kim E-K (2014) Photoacoustic imaging of breast microcalcifications: a preliminary study with 8-gauge core-biopsied breast specimens. Woloschak GE, ed. PLoS ONE 9:e105878.

Kondo M, Kobayashi K, Ohkura M, Nakai J, Matsuzaki M (2017) Two-photon calcium imaging of the medial prefrontal cortex and hippocampus without cortical invasion. Elife 6:592.

Krnjević K (1997) Role of GABA in cerebral cortex. Can J Physiol Pharmacol 75:439–451.

Lauritzen M, Jørgensen MB, Diemer NH, Gjedde A, Hansen AJ. Persistent oligemiaof rat cerebral cortex in the wake of spreading depression. Ann Neurol. 1982 Nov; 12(5):469-74. PubMed PMID: 7181451.

Li W, Chen R, Lv J, Wang H, Liu Y, Peng Y, Qian Z, Fu G, Nie L (2018) In Vivo Photoacoustic Imaging of Brain Injury and Rehabilitation by High-Efficient Near-Infrared Dye Labeled Mesenchymal Stem Cells with Enhanced Brain Barrier Permeability. Adv Sci (Weinh) 5:1700277–11.

Liu Y, Yang Y, Sun M, Cui M, Fu Y, Lin Y, Li Z, Nie L (2017) Highly specific noninvasive photoacoustic and positron emission tomography of brain plaque with functionalized croconium dye labeled by a radiotracer. Chem Sci 8:2710–2716.

Luke GP, Yeager D, Emelianov SY (2011) Biomedical Applications of Photoacoustic Imaging with Exogenous Contrast Agents. Ann Biomed Eng 40:422–437.

McCormick DA (1989) GABA as an inhibitory neurotransmitter in human cerebral cortex. Journal of Neurophysiology 62:1018–1027.

Medina-Ceja L, Pardo-Peña K, Morales-Villagrán A, Ortega-Ibarra J, López-Pérez S (2015) Increase in the extracellular glutamate level during seizures and electrical stimulation determined using a high temporal resolution technique. BMC Neurosci 16:11.

Moon H, Kang J, Sim C, Kim J, Lee H, Chang JH, Kim H (2015) Multifunctional theranostic contrast agent for photoacoustics- and ultrasound-based tumor diagnosis and ultrasound-stimulated local tumor therapy. Journal of Controlled Release 218:63–71.

Moon J-M, Thapliyal N, Hussain KK, Goyal RN, Shim Y-B (2018) Conducting polymer-based electrochemical biosensors for neurotransmitters: A review. Biosens Bioelectron 102:540–552.

Nie L, Cai X, Maslov K, Garcia-Uribe A, Anastasio MA, Wang LV (2012) Photoacoustic tomography through a whole adult human skull with a photon recycler. J Biomed Opt 17:110506.

Okubo Y, Sekiya H, Namiki S, Sakamoto H, Iinuma S, Yamasaki M, Watanabe M, Hirose K, Iino M (2010) Imaging extrasynaptic glutamate dynamics in the brain. Proceedings of the National Academy of Sciences 107:6526–6531.

Paxinos G, Watson C (2014) The Rat Brain in Stereotaxic Coordinates, Seventh edition. Elsevier Academic Press. Available at: https://books.google.com/books?id=FuqGAwAAQBAJ&printsec=frontcover#v=onepage&q&f=false.

Petersen CC, Sakmann B (2001) Functionally independent columns of rat somatosensory barrel cortex revealed with voltage-sensitive dye imaging. J Neurosci 21:8435–8446.

Petersen CCH, Grinvald A, Sakmann B (2003) Spatiotemporal Dynamics of Sensory Responses in Layer 2/3 of Rat Barrel Cortex Measured In Vivo by Voltage-Sensitive Dye Imaging Combined with Whole-Cell Voltage Recordings and Neuron Reconstructions. Journal of Neuroscience 23:1298–1309.

Rao B, Zhang R, Li L, Shao J-Y, Wang LV (2017) Photoacoustic imaging of voltage responses beyond the optical diffusion limit. Sci Rep 7:2560.

Roberts S, Seeger M, Jiang Y, Mishra A, Sigmund F, Stelzl A, Lauri A, Symvoulidis P, Rolbieski H, Preller M, Deán-Ben XL, Razansky D, Orschmann T, Desbordes SC, Vetschera P, Bach T, Ntziachristos V, Westmeyer GG (2018) Calcium Sensor for Photoacoustic Imaging. J Am Chem Soc 140:2718–2721.

Sachdev RNS, Krause MR, Mazer JA (2012) Surround suppression and sparse coding in visual and barrel cortices. Front Neural Circuits 6:43.

Sherman AD, Hegwood TS, Baruah S, Waziri R (1991) Deficient NMDA-mediated glutamate release from synaptosomes of schizophrenics. Biol Psychiatry 30:1191–1198.

Szabo GG, Du X, Oijala M, Varga C, Parent JM, Soltesz I (2017) Extended Interneuronal Network of the Dentate Gyrus. Cell Rep 20:1262–1268.

Taube JS, Schwartzkroin PA (1987) Hyperpolarizing responses to application of glutamate in hippocampal CA1 pyramidal neurons. Neuroscience Letters 78:85–90.

Voets NL, Hodgetts CJ, Sen A, Adcock JE, Emir U (2017) Hippocampal MRS and subfield volumetry at 7T detects dysfunction not specific to seizure focus. Sci Rep: 1–14.

Wang LV, Hu S (2012) Photoacoustic tomography: in vivo imaging from organelles to organs. Science 335:1458–1462.

Wang X, Pang Y, Ku G, Xie X, Stoica G, Wang LV (2003) Noninvasive laser-induced photoacoustic tomography for structural and functional in vivo imaging of the brain. Nat Biotechnol 21:803–806.

Weber J, Beard PC, Bohndiek SE (2016) Contrast agents for molecular photoacoustic imaging. Nat Meth 13:639–650.

Wu M, Springeling G, Lovrak M, Mastik F, Iskander-Rizk S, Wang T, van Beusekom HMM, van der Steen AFW, Van Soest G (2017) Real-time volumetric lipid imaging in vivo by intravascular photoacoustics at 20 frames per second. Biomed Opt Express 8:943–953.

Yao J, Maslov KI, Wang LV (2012) In vivo Photoacoustic Tomography of Total Blood Flow and Potential Imaging of Cancer Angiogenesis and Hypermetabolism. Technol Cancer Res Treat 11:301–307.

Young AM, Bradford HF (1991) N-methyl-D-aspartate releases excitatory amino acids in rat corpus striatum in vivo. J Neurochem 56:1677–1683.

Zhang HF, Maslov K, Stoica G, Wang LV (2006) Functional photoacoustic microscopy for high-resolution and noninvasive in vivo imaging. Nat Biotechnol 24:848–851.

Zhang HK, Yan P, Kang J, Abou DS, Le HND, Jha AK, Thorek DLJ, Kang JU, Rahmim A, Wong DF, Boctor EM, Loew LM (2017) Listening to membrane potential: photoacoustic voltage-sensitive dye recording. J Biomed Opt 22:045006.

Zhang P, Li L, Lin L, Hu P, Shi J, He Y, Zhu L, Zhou Y, Wang LV (2018) High-resolution deep functional imaging of the whole mouse brain by photoacoustic computed tomography in vivo. J Biophoton 11:e201700024–e201700026.